A quantitative analysis of surface deformation by stick/slip atomic force microscopy

Kerssemakers, J. ; de Hosson, J. TH. M.

Published in:
Journal of Applied Physics

DOI:
10.1063/1.366541

A quantitative analysis of surface deformation by stick/slip atomic force microscopy

J. Kerssemakers and J. Th. M. De Hosson[a)]
Department of Applied Physics, Materials Science Center, University of Groningen, Nijenborgh 4, 9747 AG Groningen, The Netherlands

(Received 5 March 1997; accepted for publication 10 July 1997)

This article presents a quantitative determination of static deformation at a nanometer scale of a surface caused by the tip of an atomic force microscope. An analysis of cantilever displacements while in contact with the surface leads to a directly measurable dimensionless parameter which is well sensitive to surface deformation. The method is specifically aimed at stick/slip friction measurements like on layered compounds, like TiS_2 or on a relatively rigid surface of an ionic crystal, in this study NaCl [100]. Stick/slip friction images offer a possibility to investigate details of strain-dependent deformation. The observed deformation in TiS_2 could play an important role in the occurrence of strong stick/slip friction in this and other layered materials. © *1997 American Institute of Physics.* [S0021-8979(97)03720-1]

I. INTRODUCTION

At a macroscopic scale friction is a smooth and usually a linear function of the applied load. This is caused by the large number of microcontacts which are continuously made and broken during sliding. In principle, from detailed observation of single-asperity sliding we could infer the basics of macroscopic friction. Atomic force microscopy (AFM) or more specifically frictional force microscopy (FFM) offers a possibility for examining such a single-asperity system in detail. With FFM the lateral movements of a needle tip, of a radius of 20–40 nm, along a surface can give some striking effects. Well known is the occurrence of highly lattice-coherent stick/slip on virtually all substrates with a high stiffness anisotropy.[1–4] Resembling a stack of loosely bound molecular layers, these substrates produce a friction image that reflects the periodicity of the surface lattice. In particular the insensitivity of the coherence to tip shape and sliding speed is noteworthy, although details in the image do change. The description of this two-dimensional stick/slip friction itself is rather complete.[1,2] Presently, we investigate the link of the stick/slip properties of any surface to material properties. One of these properties, the anisotropy of bulk stiffness, has been known to be strongly linked to stick/slip friction: the more the material structure will be of a layered character, the more it will have a tendency to display stick/slip friction.

Our goal is to study quantitatively the lateral deformation of a substrate *during* a stick/slip event. Reliable methods of measuring lateral deformation have been presented by Carpick *et al.*[5,6] and Lantz *et al.*[7] These methods rely on measuring the ratio of amplitudes of lateral strain and cantilever response. For small deformations, this ratio is constant and can well be described by Hertzian contact mechanics as has been experimentally verified.[6,7] For large deformations the concept of continuous, sliding friction can be described with Hertzian contact in the presence of capillary[8,9] or adhesive[7,10,11] forces. However, stick/slip friction forms a transition between static contact and sliding friction. Because of the catastrophic nature of a slip event, this intermediate behavior cannot fully satisfactorily, i.e., on an atomic scale, be described with the aforementioned methods. We are interested in the lateral stiffness at small strains as well as the stiffness just before a slip takes place when the contact area is fully strained. For stick/slip on ionic crystals for instance, the latter stiffness can be greatly reduced, as we will show.

To measure this stiffness, a fully calibrated probe is essential. This means the detector response as well as the actual cantilever stiffness should be known. Carpick *et al.* have proposed an *in situ* method independent of cantilever or detector type, yielding a ratio of signal yield for lateral and normal movements.[7] Although this proved to be very reliable, we prefer an *ex situ* method based on an analysis of Neumeister *et al.*[12] Despite the larger expected errors, such an analytical method more clearly links possible force components and cantilever movements, which for our purpose of studying stick/slip is preferable. Moreover, with an *ex situ* method no assumptions on tip–sample contact deformation as described above, need to be made. As we will show, the method yields a corresponding sensitivity ratio, as well as expressions for the cantilever stiffness in any configuration. Due to instrumental restrictions we are only able to measure the deflection along the cantilever length. Therefore the calibration will be performed along this length axis. Although it is more usual to measure friction along the torsional axis of the cantilever, it can be shown that when stick/slip is present, the cantilever signal is primarily frictional in all directions.[2]

It is useful to validate our method on substrates covering a wide range of stiffness anisotropy in combination with stick/slip friction. For this purpose we took substrates of the transition metal dichalcogenide compound TiS_2 and ordinary rock salt NaCl [100].

II. THEORETICAL DESCRIPTION

Stick/slip friction

With two-dimensional stick/slip friction, discrete points between which the tip jumps, correspond to lattice sites of

a)Author to whom all correspondence should be addressed. Electronic mail: hossonj@phys.rug.nl

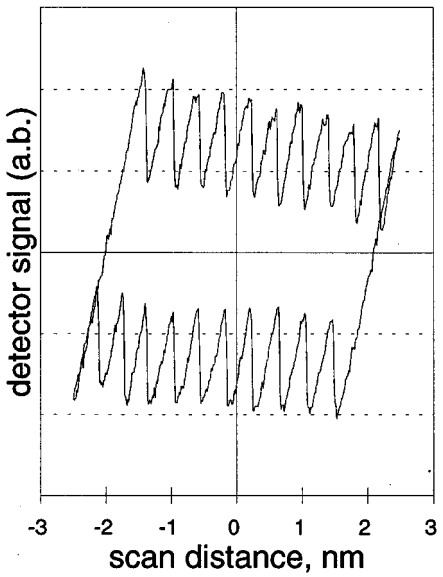

FIG. 1. A typical forward (lower) and backward (upper) friction loop of a $\langle 1120 \rangle$ line scan on NbS_2. Stick and slip parts are clearly visible as linear parts alternated by steep jumps.

the substrate. Although the contact area of the tip is normally much larger than one atom, the periodicity of the alternating stick and slip phases is still that of the substrate, provided that we only consider next-neighbor jumps. In an earlier article, we proposed a model that describes correctly the observed friction images.[2] In this model, the model probe is only allowed to jump instantaneously from one lattice site to another. Once stuck again, the cantilever strains until the next jump takes place. This jump occurs as soon as the pulling force exceeds a certain level, which corresponds to a maximum displacement length in the model. For this length we took the same value in all directions, resulting in a maximum displacement circle. The cantilever tip never strains more from its relaxed position than the radius of this circle. One important feature of our model is, that the cantilever is always assumed to strain in the direction of the pulling force, i.e., there is no buckling. Each scan line will be composed of a series of jumps, globally in the direction of the scan line. Previously we analyzed the details of these jump sequences by making a transformation from the substrate to the cantilever coordinates, the latter with the origin in the cantilever base.

Within the same model description we will not focus here on the jump events but on the straining part of the signal, that is to say on the stick phase. In actual friction loops, the stick and slip events can clearly be recognized as linear parts and sharp drops, respectively. This is displayed in Fig. 1. Only when there is no buckling of the cantilever, the slope of the signal in the sticking phase will reflect a strong indication that lateral stick/slip occurs, i.e., a sinusoidal variation of the slope with scan direction. This is so because the detection signal only reflects one component of the strain. The direction of this component depends on the detector-cantilever-laser configuration and does not lie necessarily along the x axis. All possible cantilever positions together result in a linear signal of intensity through the origin of zero straining. This means that, given an equal amount of straining, the resulting derivative of the signal will form a sinusoidal function of the scan direction α, according to

$$\text{sensitivity} \equiv \frac{d(\text{signal})}{d(\text{displacement})} = A \sin(\alpha - \alpha_0).$$

A sinusoidal function proves that any nonfrictional part in the signal is negligibly small. The amplitude A is proportional to the maximum signal sensitivity for a cantilever torque, given a specific configuration. However, it need not be equal to it for the following reason. So far the strain was only thought to be restricted to the cantilever, whereas the slip threshold was a matter of tip–surface interaction. Now we go one step further and we consider significant deformation underneath the surface top layer. The model spring is then composed of the cantilever in series with an *a priori* unknown surface deformation mechanism. Like the straining, the jumping or relaxing will be distributed over cantilever and substrate. Although the stick/slip model holds equally well, the difference is that of the total strain, only the straining of the cantilever will be detected, whereas the deformation of the surface is hidden. Given an equal total displacement the signal yield will be lower. The maximum signal yield and corresponding sensitivity will only be reached with an infinitely stiff substrate.

When we are able to predict the cantilever signal yield per lateral tip displacement or lateral sensitivity, any discrepancy of the actual sensitivity with the theoretical maximum can in principle be used to measure directly the surface stiffness with respect to the lateral cantilever stiffness. Especially on layered substrates, the values of surface and cantilever stiffness could fall within the same order of magnitude, making the sensitivity decrease significant.[5,7]

Quantifying cantilever behavior

Static deformation of the cantilever itself has been analyzed in detail, for bar- as well as V-shaped models.[12–17] As argued before, for our purpose we prefer an analytical model. The detailed cantilever analysis presented by Neumeister *et al.*[12] was taken as a starting point. For a detailed analysis see the Appendix. The cantilever signal is directly proportional to the angle change θ at the tip of the cantilever, see Fig. 5. The expressions derived in the Appendix yield the signal response sensitivities

$$\left[\frac{d\theta}{dL}\right] \quad \text{and} \quad \left[\frac{d\theta}{dY}\right], \tag{1}$$

where dL and dY correspond to lateral and vertical scanner movements, respectively (Fig. 5). The actual signal yield in V per angle change is not known, but it should be the same for both lateral and vertical sensitivities. Therefore we may circumvent this unknown yield by taking the ratio of these two sensitivities.[6] In this way we obtain a dimensionless constant R, the predicted value of which is given by

$$R \equiv \frac{d\theta/dx_s}{d\theta/dy_s} = \left| \frac{R_{\max}}{1 + \lceil C_s / C_{\text{eff}} \rceil} \right|. \tag{2}$$

For details on Eq. (2) reference is made to the Appendix. The compliance C_{eff} expresses an effective lateral compliance of

TABLE I. Properties and sensitivity ratio R of the cantilever used.

Geometry (bar shape)			
Base-tip length	L	125.1 ± 0.1 μm	
Beam width	w	22.5 ± 0.1 μm	
Beam thickness	t	0.5 ± 0.1 μm	
Tip length	h	3.5 ± 0.1 μm	
Contact angle	α	$12.5 \pm 1.5°$	
Bulk E modulus[a,b]	E	304 GPa	
Poisson's ratio[a]	ν	0.24	
Compliances	|Value|	Stiffness	|Value| N/m
$C_\theta = L/Ewt^3$	1.46×10^8	$[C_\theta H^2]^{-1}$	486 ± 120
$C_z = L^3/3Ewt^3$	0.76	$[C_z]^{-1}$	1.31 ± 0.33
$C_{\theta z} = L^2/2Ewt^3$	9.15×10^3	$[C_{\theta z} H]^{-1}$	29.1 ± 7.3
C_{eff}	2.18×10^{-3}	$[C_{\text{eff}}]^{-1}$	459 ± 110
Sensitivity ratio			
$R_{\max}$	$\left[\frac{\Delta R}{\Delta \alpha}\right]_{\alpha=12.5}$	$\left[\frac{\Delta R}{\Delta H}\right]_{H=4.0}$	
20.8 ± 0.5	0.25	0.5	

[a]J. M. Neumeister and W. A. Ducker, Rev. Sci. Instrum. **65**, 2527 (1994).
[b]T. J. Senden and W. A. Ducker, Langmuir **10**, 1003 (1994).

the cantilever. Furthermore, as a first approximation of substrate lateral elasticity, C_s is taken being the substrate compliance. This C_s will obviously influence the displacement of the cantilever. Considering the low vertical stiffness of the cantilever despite the rotation R we assume the substrate being rigid in directions perpendicular to the surface.[5] The value of C_s allows us to distinguish between substrates which are almost isotropic in stiffness, like ionic crystals, and those who are anisotropic, such as most layered materials. For rigid substrates, $C_s = 0$. Both calculated and measured sensitivities, although different in physical units, should result in the same value of R. The dimensions and properties of the cantilever used are given in Table I.

As can be inferred from Eq. (2), R is sensitive to the substrate compliance C_s, in a broad range of two orders of magnitude around the effective lateral cantilever compliance. Expressed in stiffness C^{-1} this value is of order 10^2 N/m. Layered substrates could yield surface stiffness well within this range.[5,7]

The largest uncertainties in R result from the third-order dependence of the cantilever stiffness to its beam thickness[12] and of the effective value of the E modulus of the cantilever material[18] (see Table I). To a lesser degree the exact location of the tip at the end of a V-shaped cantilever[12] affects R. However, a useful property of R is, that at infinite substrate stiffness the influence of the first two approaches zero, and only the total tip height H remains of importance. This offers us the possibility to check our predictions on rigid substrates.

III. EXPERIMENT

In the derivation of the sensitivity ratio R, we consider only the deflection and bending of an imaginary point right at the base of the tip pyramid. In reality the laser spot reflects from a large area at the cantilever end. The actual sensitivity is the integrated product of reflecting light with the local

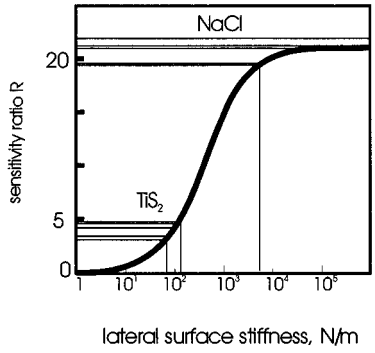

FIG. 2. The ratio of lateral vs vertical sensitivity depends on the lateral surface stiffness, given the same cantilever configuration. The predicted curve is for a 12.5° contact angle of the cantilever. We see the measured values of R lead to a low lateral stiffness for TiS_2 of $(1.1 \pm 0.2) \times 10^2$ N/m, while on NaCl we see agreement of the measured values with the predicted R on a rigid surface.

bending. Not only is this bending nonlinear along the cantilever,[6] but also different for different combinations of bending moment and loading force.[13] The finite spot size effect has a different influence on lateral and vertical sensitivities. Therefore, we did not preferably tune the AFM to maximum light yield, but instead to a maximum ratio of vertical sensitivity and total signal yield. Experimentally it was verified that this protocol puts the center of the laser spot within a few micrometers of the desired place. It was found that the intensity profile of the laser spot has a half-width of about 25 μm. Following the above, the reflected light comes mainly from the last 20 μm of the cantilever. We measured our cantilevers carefully in a Philips XL30 FEG low voltage scanning electron microscope (SEM) and inserted the geometry obtained in the expression of Eq. (2) for R. The resultant curve is depicted in Fig. 2 for a contact angle of 12.5°. The value of $R_{\max}$ (see Table I) is predicted to be 20.8 ± 0.5. The lower part of the curve should be taken as an estimate because of the high uncertainties in the actual cantilever compliances.

TiS_2 consists of layers of Ti atoms surrounded by sulfur atoms. The surface lattice reflects the hexagonal coordination of the sulfur atoms, spaced 0.34 nm apart in the surface plane. The layers are only weakly bonded by van der Waals forces. Considering the differences between intra- and interlayer bonding, the substrate can be regarded as a stacking of loosely bonded and slightly deformable atomic sheets. NaCl [100] reflects a cubic fcc lattice with a unit cell spacing of 0.56 nm and a nearest neighbor (Cl–Cl) spacing of 0.40 nm. Each surface atom is connected to its neighbors by ionic bonds, as strongly in the upper layer as with its second-layer nearest neighbor. In terms of stiffness, the largest difference between the two materials will occur parallel to the surface plane. On both substrates it is possible to obtain friction images with typical stick/slip characteristics. Normally the number of available jump sites is equal to the number of nearest-surface neighbors. Therefore the symmetry difference between the lattices of TiS_2 (hexagonal) and NaCl (fcc cubic) has a profound influence on the slip behavior. However, as long as we take the maximum allowed tip strain to

be independent of orientation, like in our earlier jump analysis,[2] the sticking phase behavior is independent of lattice symmetry. Like in the jump analysis we obtained sets of scan lines at different scanning directions on TiS_2 and NaCl in ambient air. To do this in a compact way, we modified the scan-type of our Nanoscope-II optical-lever AFM. The original grid scan was transformed into a polar scan, in which each scan line is scanned at a slightly different orientation, similar to the work of O'Shea.[4] In our setup, however, the resulting 400 scan lines are still imaged in 400×400 Cartesian coordinates as shown in Fig. 3. This simplifies angular dependent data processing. The great experimental advantage of polar scans is that all dependency of the signal on scan direction is compressed in one single data set and therefore time saving. In the polar maps we recognize the typical saw tooth line scans associated with stick/slip friction. Apart from the actual contrast, for the jump transition patterns we discern a sixfold periodicity in the TiS_2 map and a fourfold one in the NaCl map which correspond to hexagonal and cubic lattices, respectively. Measuring along the main axes of the lattice, we find from these images a jump spacing of (0.40 ± 0.01) nm for NaCl and of (0.34 ± 0.01) nm for TiS_2. This is consistent with nearest-neighbor jumps on the respective surface lattices. Clearly visible are also qualitative differences between the two friction images: the stick and slip phases are sharper and more regular in TiS_2, than in NaCl along the scan lines. On the other hand, the signal slope seems to be much higher in NaCl, as can be seen in the scan profiles in Fig. 3 where both profiles are shown at the same scale. This mean slope expresses the lateral sensitivity which we need to determine the sensitivity ratio R. The periodic stick and slip traject itself is not very useful to obtain this lateral sensitivity. In that case second-order terms in the substrate compliance C_s can come of influence, which is probably happening on the NaCl surface. This results in a decreased sensitivity of the stick phase signal during the scan compared to that at the start of a scan. To avoid this possible second-order perturbation we take only the first part of each scan line, since this bears the best approximation of a static tip contact. For the purpose of validating our method, we measured the slope of only the first 0.37 nm of all scan lines, which normally is shorter than the distance the tip needs to travel before slipping takes place. We did this by simple linear regression of this part over intervals of 0.02–0.03 nm.

The resulting points were collected in a two-dimensional histogram of counts as a function of slope and scan angle. Along each angle of scan direction, the maximum or most encountered slope was taken as the representative lateral sensitivity for that particular angle. Figure 4 shows the total compilation of sensitivities thus obtained for two measurements on NaCl and on TiS_2. The cantilever and tuning was unchanged for both curves, making them directly comparable. Both curves fit accurately to a sinusoidal function, having the same phase but differ in amplitude. As has been explained before, this proves that both measurements reflect lateral friction, and secondly that in both cases no buckling of the cantilever appears. This means that the deformation process can indeed be interpreted as a straight series of springs in all directions, which keeps our simple model along the main axis of the cantilever valid. Thirdly, the difference in amplitude points to a proportional difference in R. As all other parameters determining Eq. (2) (see the Appendix) re-

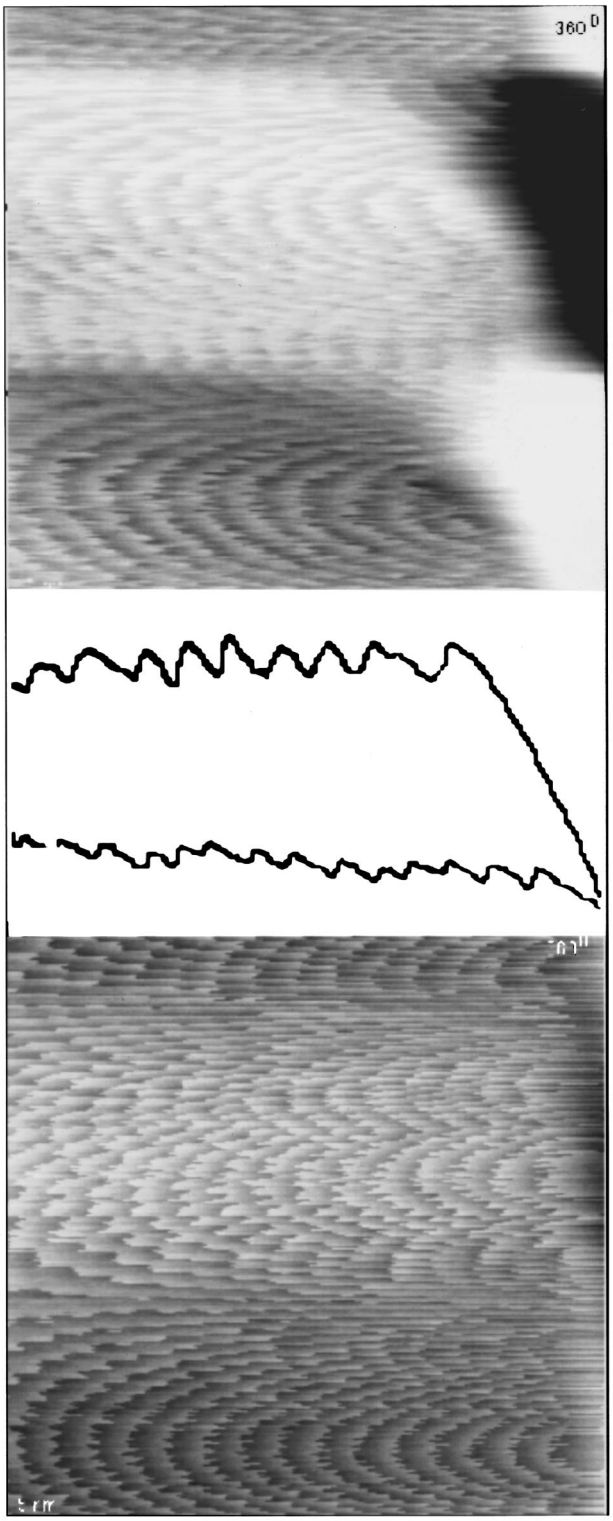

FIG. 3. Polar scans on TiS_2 (lower) and NaCl (upper). Each horizontal line is a scan line of 5 nm. The scan direction varies from 0° to 360° along the y axes. From these pictures, the stick/slip system can easily be interpreted in terms of lattice symmetry and orientation which affect the jump phase, but also aspects of the sticking phase can be measured: from the line profiles (center) we see the static friction reflects a much higher slope in the case of NaCl than with TiS_2. See also Fig. 4.

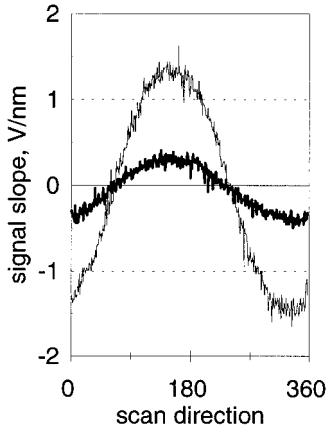

FIG. 4. The slope as a function of scan direction, as obtained from the first 0.37 nm of the scans in Fig. 3. The two sinusoidal shapes are a proof for lateral friction in both cases, TiS_2 (thick curve) and NaCl (thin curve), as they reflect the visible component of a constant frictional signal by a single-split photodetector. The amplitude difference between the two (see also Fig. 3) shows up clearly. This gives clues on surface deformation present with TiS_2, causing a decrease in cantilever bending for the same displacement of the cantilever, relative to NaCl.

main unchanged or are of insignificant influence, this implies a clear difference in surface stiffness for NaCl and TiS_2. By dividing the amplitudes by the vertical sensitivities, we finally obtain the respective sensitivity ratios R. For TiS_2 we found a value of (4.0 ± 0.5) for five scans, while for NaCl we found a value of (20.7 ± 1.0) for the same number. In Fig. 2 we show that via the predicted dependence of R for this cantilever, we get quantitative information on the lateral stiffness in both samples. For the cantilever used, (see Table I) a specific expression for the stiffness k_s of the surface is

$$k_s = k_{\mathrm{eff}}\left(\frac{1}{(R_{\max}/R)-1}\right] = \frac{460}{[(20.8/R)-1]}. \tag{3}$$

As the sensitivity of k_s goes to infinity for values of R close to the maximum, only the value of R found on TiS_2 will yield a value for the stiffness, of $(1.1\pm0.2)\times10^2$ N/m. This is a value comparable to similar experiments on mica[5] and $NbSe_2$.[7] The case of NaCl shows an average value of R of (20.7 ± 1.0) which shows no significant deviation from the value of (20.8 ± 0.5) expected for $R_{\max}$ (see Table I). This implies that in these experiments, there seems to be no presence of tip deformation as described in the work of Lantz.[7] We conclude from this that the predicted upper value for R agrees well with that expected on a completely rigid surface, by a rigid tip.

IV. DISCUSSION

Using an *ex situ* calibration method, we measured a stiffness of a surface in lateral directions for subnanometer deformations. The relatively low stiffness on an anisotropic material like TiS_2 is not very surprising. From the point of view of stick/slip friction, this low stiffness gives us a clue about the origin of stick/slip friction on layered substrates when using a relatively stiffer AFM cantilever. In most explanations for the occurrence of sharp, saw-tooth-like stick/slip friction, the sliding planes of tip and surface should be commensurate, a fact which has been recognized and simulated in the past. Any deviation from a commensurate fit should strongly weaken the sharpness of the stick/slip.[19] Contrary to this, the actual stick/slip observed on layered substrates is rather insensitive to the tip topography. However, surface deformation may solve this seeming paradox. From Fig. 4, it is easy to see that about 4/5 of the total deformation on TiS_2 takes place between tip and surface or underneath this, as only 1/5 of the piezo movement is reflected in the cantilever bending during the stick phase. From literature, this ratio seems not unrealistic.[5,7] Furthermore, the tip–surface potential cannot account for a tip–surface glide of more than one nearest-neighbor distance during the sticking phase. The static friction on layered substrates regularly exceeds this distance without any observed qualitative changes, as can be seen in Fig. 1. The only alternative left is a significant movement underneath the upper layer, accounting for most of the deformation. Such a subsurface movement makes the need for a commensurate fit between tip and surface latticeless: the straining of the tip–lattice interface becomes less significant relative to the subsurface deformation, while the lower the stiffness of the latter, the lower the forces in the tip–surface interface get for the same displacement. Thus, nonlinear tip–surface glide during the stick phase causes relatively less deviations from linear straining on the *total* deformation of cantilever, contact area, and subsurface contributions. In summary: the mere introduction of an easily deformable subsurface ''sharpens'' stick/slip friction, given the same tip–surface potential. Qualitatively, this relative decrease of nonlinearity can be measured in the polar maps, see Fig. 3. On NaCl, the most encountered slope during the scan was measured to be (0.76 ± 0.04) V/nm, on average 3.6 times lower than the slope which was measured at the start of the scan lines, the latter agreeing well with the theoretical maximum. In the case of TiS_2, this same factor was only 1.02. Consequently, on NaCl the glide in the tip–substrate interface during the sticking phase must be relatively significant, in contrast to the situation on TiS_2. In combination with the observed lateral rigidity and weakness on NaCl and TiS_2, respectively, this supports the idea of deformation-assisted stick/slip friction on layered substrates. From the sharp saw tooth in TiS_2 we see that the stick phases are linear in the TiS_2 case and we suggest therefore that the actual contact area of the tip does not change too much during straining. In that case the area surrounding the tip and the amount of bonding of the upper layer to the second layer together cause the resistance to deformation, making application of extended Hertzian models possible.[9,10] In the case of nonlinear stick/slip as observed on NaCl, our method offers the possibility to study the effect of lateral strain on stiffness.[20]

V. CONCLUSIONS

We were able to measure local lateral stiffnesses of TiS_2 and NaCl surface areas. This was possible by devising a reasonable accurate description of an arbitrary cantilever-tip-surface configuration. This descriptions aims specifically at analyzing strain-dependent stiffness encountered during

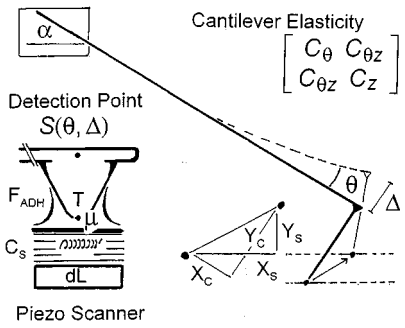

FIG. 5. Model for a cantilever in contact with a surface. The cantilever itself is described with a compliance matrix C_{ij}. Two coordinate systems $(_{s,c}, Y_{s,c})$ are used, orthogonal to the substrate and cantilever, respectively. The tip–sample interaction, at point T, is described with an adhesion force F_{adh}, a friction coefficient μ, and a lateral substrate compliance C_s. Detection of the cantilever movement is in point S, expressed in bending angle θ and deflection Δ.

stick/slip friction. The accuracy of this description was supported by the close correspondence of prediction and measurement of the cantilever deformation on a relatively rigid surface, NaCl [100]. The simultaneous observation of strongly linear sticking phases and significant subsurface deformation on TiS_2 contrary to NaCl, suggest that this deformation is a direct cause for the well-known strong stick/slip friction on layered substrates.

ACKNOWLEDGMENTS

The work described in this article is part of the research program of the Foundation for Fundamental Research on Matter (FOM-Utrecht) and has been made possible by financial support from the Netherlands Foundation for Technical Sciences (STW-Utrecht).

APPENDIX: DERIVATION OF SIGNAL RESPONSE

The calculation of the lateral sensitivity corresponds to the calculations of the respective changes in angle θ of the detection point S for movements of the scanner piezo in lateral and vertical directions (see Fig. 5). The piezo is thought to be connected to the tip point T by a lateral substrate spring with compliance C_s and a sliding contact at point T with a dynamic friction coefficient μ. On the point of the tip works the cantilever loading force F_{load} and capillary force F_{adh} both perpendicular to the surface of the substrate. These are balanced by the substrate exerting the opposite force on the tip. In the lateral direction the same holds: the lateral force F_{lat} deforming the sample equals to the lateral components of the cantilever. The total vertical force $F_{\text{vert}} = F_{\text{load}} + F_{\text{adh}}$ determines this lateral force as soon as the tip, for any movement, exceeds the static friction and starts sliding,

$$F_{\text{lat}} = \mu(F_{\text{load}} + F_{\text{adh}}). \tag{A1}$$

This sliding also will occur when the piezo is moved over relatively large vertical distances used when calibrating an AFM. On the other hand, the lateral sensitivity will be taken as the response measured before any sliding occurs, so that the tip contact is without any allowed sliding, although the substrate still can deform of course. Both cases, a sliding and a surface-fixed tip, can be simply described within the same model, as will be shown in the following.

Any force system on the cantilever can easily be described by a bending moment M and a force N, the latter perpendicular to the cantilever plane, see Fig. 5. M and N are linked to the above forces as follows:

$$\begin{pmatrix} F_{\text{lat}} \\ F_{\text{load}} \end{pmatrix} = \begin{bmatrix} \sin(\alpha) & \cos(\alpha) \\ \cos(\alpha) & -\sin(\alpha) \end{bmatrix} \begin{bmatrix} N \\ M/H \end{bmatrix}, \tag{A2}$$

where H is the tip height h plus half the cantilever thickness t: $H = (h + t/2)$. From Eqs. (A1) and (A2) we can eliminate M, and use the result of Neumeister *et al.*,[12]

$$\begin{pmatrix} \theta \\ \Delta \end{pmatrix} = \begin{pmatrix} C_\theta & C_{\theta z} \\ C_{\theta z} & C_z \end{pmatrix} \begin{pmatrix} M \\ N \end{pmatrix}, \tag{A3}$$

where the C_{ij} are the various cantilever compliances, depending on geometrical and mechanical properties of the cantilever only (see also Table I).

Lateral sensitivity

Equation (A3) can be used to express the deflection Δ and angle change θ in only the moment M as variable, as this moment forms the highest contribution to the lateral forces,

$$\begin{pmatrix} \theta \\ \Delta \end{pmatrix} = \begin{bmatrix} C_\theta & C_{\theta z} \\ C_{\theta z} & C_z \end{bmatrix} \left[M \begin{pmatrix} 1 \\ O_\mu \end{pmatrix} - F_{\text{adh}} \begin{pmatrix} 0 \\ I_\mu \end{pmatrix} \right], \tag{A4}$$

where

$$O_\mu = \left[\frac{\cos(\alpha) + \mu \sin(\alpha)}{\mu \cos(\alpha) - \sin(\alpha)} \left(\frac{1}{H} \right) \right]$$

and

$$I_\mu = \left[\frac{\mu}{\mu \cos(\alpha) - \sin(\alpha)} \right].$$

From Eq. (A4), changes in angle θ and deflection Δ are expressed in the differential equations

$$d\theta = (C_\theta + C_{\theta z} O_\mu) dM, \tag{A5a}$$

$$d\Delta = (C_{\theta z} + C_z O_\mu) dM \tag{A5b}$$

in which we assume a constant adhesion force. Though this need be true in general, during stick/slip friction this seems reasonable, as the vertical displacement of the tip relative to the substrate during a slip is small. Thus, for $dM \neq 0$, as long as Eq. (A1) holds we have

$$\frac{d\Delta}{d\theta} = C_\mu, \tag{A6a}$$

where

$$C_\mu = \left[\frac{C_{\theta z} + C_z O_\mu}{C_\theta + C_{\theta z} O_\mu} \right]. \tag{A6b}$$

The lateral sensitivity is defined as $d\theta/dl$ where dl is a lateral movement of the piezo scanner. When the tip does not slide relative to the surface, this movement equals $d(x_s + u_s)$, the tip and substrate displacement, respectively.

For dx_s, we use (see Fig. 5)

$$\begin{pmatrix} x_s \\ y_s \end{pmatrix} = \begin{pmatrix} \cos(\alpha) & \sin(\alpha) \\ -\sin(\alpha) & \cos(\alpha) \end{pmatrix} \begin{pmatrix} x_c \\ y_c \end{pmatrix}$$

and

$$\begin{pmatrix} x_c \\ y_c \end{pmatrix} = \begin{pmatrix} H\theta + f(\Delta) \\ \Delta \end{pmatrix}. \tag{A7}$$

The function $f(\Delta)$ expresses the movement along the cantilever plane of the point S due to the bending of the cantilever. For a 115 μm long triangular cantilever, this contribution in x_c may not be neglected when y_c exceeds a few hundreds of nm. In this derivation however we will not consider it further because of the relative magnitudes of displacements we encounter when determining lateral and vertical sensitivities. Then, Eq. (A7) allows us to express dx_s and dy_s in $d\theta$ and $d\Delta$,

$$dx_s = H\ \cos(\alpha) d\theta + \sin(\alpha) d\Delta, \tag{A8a}$$

$$dy_s = -H\ \sin(\alpha) d\theta + \cos(\alpha) d\Delta. \tag{A8b}$$

Moving the piezo dl laterally, while keeping the tip on the surface, imposes the condition $dy_s = 0$. For the latter, using Eq. (A6) and (A8b), this gives

$$C_\mu = H\ \tan(\alpha) \vee \tag{A9a}$$

$$dN = 0. \tag{A9b}$$

Equation (A9a) determines the value of μ. This cannot be combined with the general expression Eq. (A1) when μ is an independent material property. Therefore, the sliding regime corresponds to Eq. (A9b), leading to $d\theta = 0$ and $d\Delta = 0$. Equations (A1)–(A4) and (A7) then lead to a fixed relation between X_s and Y_s. This X_s expresses the distance mostly called static friction $\epsilon_0 = x_s$.[1–3] Equation (A9a) holds when the tip is fixed to the surface, and μ has no direct physical meaning though Eq. (A1) is still valid. Then Eq. (A8a) leads with Eq. (A9a) and Eq. (A6) to

$$dx_s = \left[\frac{H}{\cos(\alpha)} \right] d\theta. \tag{A10}$$

With Eqs. (A1), (A2), and (A5), we can now express the lateral force F_{lat} in terms of $d\theta$. The change in the lateral force should be equal and opposite to the change in the lateral component of the cantilever force. Using (A10) it is convenient to define an effective lateral cantilever compliance C_{eff}

$$C_{\text{eff}} \equiv \left[-\frac{dF_{\text{lat}}}{dx_s} \right]^{-1} = \left[-\left(\frac{\cos(\alpha)}{H} \right) \frac{\sin(\alpha) + O_F\ \cos(\alpha)}{C_\theta H O_F + C_{\theta z}} \right]^{-1}. \tag{A11}$$

Because we are in the fixed tip regime, the value of O_F in Eq. (A11) is determined by Eq. (A9a), and is equal to

$$O_{\mu,\text{fixed}} = O_F = \frac{C_\theta H\ \sin(\alpha) - C_{\theta z}\ \cos(\alpha)}{C_z\ \cos(\alpha) - C_{\theta z} H\ \sin(\alpha)}. \tag{A12}$$

To express du_s in $d\theta$ we use $du_s = -C_s d(F_{\text{lat}})$, where C_s is the lateral compliance of the substrate. Note du_s is expressed in $d\theta$,

$$du_s = \frac{H}{\cos(\alpha)} \left(\frac{C_s}{C_{\text{eff}}} \right) d\theta. \tag{A13}$$

Equations (A10) and (A13) result in the lateral sensitivity,

$$\frac{d\theta}{dl} = \left\{ \frac{H}{\cos(\alpha)} \left[1 + \left(\frac{C_s}{C_{\text{eff}}} \right) \right] \right\}, \tag{A14}$$

in which we clearly see the influence of the surface compliance C_s, scaling with the effective cantilever compliance C_{eff}, as we should expect.

Vertical sensitivity

For the vertical sensitivity $d\theta/dy_s$ we follow the same routine. However, now the equivalent expressions for Eq. (A5) in dN are used because the tip is sliding and therefore the moment force only gives a small contribution to θ. There exists no further restriction on μ. Analogously to the derivation in x_s, we find dy_s expressed in $d\theta$. The vertical sensitivity can be written as

$$\frac{d\theta}{dy_s} = \frac{1}{H[D_\mu\ \cos(\alpha) - \sin(\alpha)]}, \tag{A15}$$

where

$$D_\mu = \left(\frac{C_z O_\mu + C_{\theta z}}{C_{\theta z} O_\mu + C_\theta} \right) \frac{1}{H}.$$

As explained in the main text, the ratio of lateral and vertical sensitivity is a directly measurable parameter, which from Eqs. (A14) and (A15) is predicted as

$$R = \left| \frac{[D_\mu\ \cos(\alpha) - \sin(\alpha)]\cos(\alpha)}{1 + \left[\frac{C_s}{C_{\text{eff}}} \right]} \right|. \tag{A16}$$

Equation (A16) is a general result. All cantilever shapes are applicable via the various cantilever compliances C_{ij}. On an infinitely rigid substrate, R simplifies with $C_s = 0$ to

$$R_{\max} = [D_\mu\ \cos(\alpha) - \sin(\alpha)]\cos(\alpha). \tag{A17}$$

This is an upper limit for R, given the contact angle. As the constant D_μ consists of a ratio of cantilever compliances [see Eq. (A15)], this limit is insensitive to the large errors in individual compliances C_{ij} that originate from the inaccurate determination of the cantilever effective E modulus and thickness.[18] The order of magnitude of this $R_{\max}$ for commercial cantilevers will be 20–30, for bar as well V shapes. See also Table I and Fig. 2.

[1] S. Morita, S. Fujisawa, and Y. Sugawara, Surf. Sci. Rep. **23**, 1 (1996).
[2] J. Kerssemakers and J. Th. M. de Hosson, J. Appl. Phys. **80**, 623 (1996).
[3] S. Fujisawa, E. Kishi, Y. Sugawara, and S. Morita, Appl. Phys. Lett. **66**, 526 (1995).
[4] S. J. O'Shea, M. E. Welland, and T. M. H. Wong, Ultramicroscopy **52**, 55 (1993).
[5] R. W. Carpick, D. F. Ogletree, and M. Salmeron, Appl. Phys. Lett. **70**, 526 (1997).

[6] D. F. Ogletree, R. W. Carpick, and M. Salmeron, Rev. Sci. Instrum. **67**, 3298 (1996).
[7] M. A. Lantz, S. J. O'Shea, A. C. F. Hoole, and M. E. Welland, Appl. Phys. Lett. **70**, 970 (1997).
[8] U. D. Schwarz, W. Allers, G. Gensterblum, and R. Wiesendanger, Phys. Rev. B **52**, 14 976 (1995).
[9] A. Fogden and L. R. White, J. Colloid Interface Sci. **138**, 414 (1990).
[10] K. L. Johnson, K. Kendall, and A. D. Roberts, Proc. R. Soc. London, Ser. A **324**, 301 (1971).
[11] R. W. Carpick, N. Agrait, D. F. Ogletree, and M. Salmeron, J. Vac. Sci. Technol. B **14**, 1289 (1996).
[12] J. M. Neumeister and W. A. Ducker, Rev. Sci. Instrum. **65**, 2527 (1994).
[13] R. J. Warmack, X. Y. Zheng, T. Thundat, and D. P. Allison, Rev. Sci. Instrum. **65**, 394 (1994).
[14] J. E. Sader and L. White, J. Appl. Phys. **74**, 1 (1993).
[15] J. E. Sader, Rev. Sci. Instrum. **66**, 4583 (1995).
[16] J. E. Sader, I. Larson, P. Mulvaney, and L. R. White, Rev. Sci. Instrum. **66**, 3789 (1995).
[17] M. Labardi, M. Allegrini, M. Salerno, C. Frediani, and C. Ascoli, Appl. Phys. A **59**, 3 (1994).
[18] T. J. Senden and W. A. Ducker, Langmuir **10**, 1003 (1994).
[19] M. R. Sorensen, K. W. Jacobsen, and P. Stoltze, Phys. Rev. B **53**, 2101 (1996).
[20] J. W. J. Kerssemakers and J. Th. M. de Hosson (unpublished).